Elsevier Editorial System(tm) for Renewable Energy

Manuscript Draft

Manuscript Number: RENE-D-19-02921R1

Title: Dynamic response of Pelton runners: numerical and experimental analysis in prototypes

Article Type: Research Paper

Keywords: Hydropower, Pelton turbines, Dynamic response

Corresponding Author: Ms. Mònica Egusquiza,

Corresponding Author's Institution: Polytechnic University of Catalonia (UPC

First Author: Mònica Egusquiza

Order of Authors: Mònica Egusquiza; Carme Valero; David Valentín; Alexandre Presas; Eduard Egusquiza

Abstract: With the growth of new renewable energies, hydropower has become crucial to stabilize the power grid. This has led turbines to working in more extreme loads and with more start/stop sequences. Pelton turbines are subjected to strong pulsating forces during operation due to the action of high-speed water jets. Consequently, buckets present large deformations and stresses, which are aggravated when the runner enters resonance. Therefore, the dynamic response of the turbine must be thoroughly studied and the most dangerous frequencies avoided.
In this paper, a detailed analysis of the modal behavior of Pelton turbines is presented. Four prototypes have been studied for such purpose. The first one has been modeled numerically and analyzed experimentally. Following a systematic investigation, the effect on the modal shapes and the frequencies of the different parts comprising the turbine has been evaluated. The single bucket and the whole runner have been studied.
The second turbine, which is installed in the same power plant, has been analyzed to determine the effect of the mechanical design on the frequencies.
Finally, two prototypes belonging to other power plants have been studied to see the effects of the hydrodynamic design on the modal behavior.

Dynamic response of Pelton runners: numerical and experimental analysis in prototypes

Mònica Egusquiza[a]*, Carme Valero[a], David Valentín[a], Alexandre Presas[a], Eduard Egusquiza[a]

a Center for Industrial Diagnostics and Fluid Dynamics (CDIF), Polytechnic University of Catalonia (UPC), Av. Diagonal, 647, ETSEIB, 08028, Barcelona, Spain

* Correspondence: monica.egusquiza@upc.edu; Tel.: +34-934-016-715

Abstract

Worldwide electricity generation is featured by the growth of intermittent renewable energies. In this context, hydropower plays a fundamental role because it provides flexibility to the power grid and ensures its stability. The new grid requirements have led hydropower units to working under a wider range of loads and with more start/stop sequences.

Pelton turbines are the most suitable for high heads and have a large regulation capacity. In operation, the runner is impinged by high-speed water jets, and, thus, subjected to strong pulsating forces. As a consequence, the structure presents large deformations and high stresses, especially on the buckets. This situation can be much aggravated if the frequency and shape of the excitation is resonant with those of the structure. Therefore, the modal response of the turbine must be thoroughly studied and the most dangerous frequencies avoided.

In this paper, a detailed analysis of the modal behavior of Pelton turbines is presented. Four prototypes have been studied for such purpose. The first one has been modeled numerically and analyzed experimentally. Following a systematic investigation, the effect on the modal shapes and the frequencies of the different parts comprising the turbine has been evaluated. The single bucket and the whole runner have been studied.

Finally, another turbine installed in the same power plant has been analyzed to determine the effect of the mechanical design on the frequencies. In addition, two prototypes belonging to other power plants have been studied to see the effects of the hydrodynamic design on the modal behavior.

Keywords: Hydropower, Pelton turbines, dynamic response

1. Introduction

At present, new renewable energies are experiencing a strong development. These are predominantly constituted by wind power stations and solar farms, which, despite their environmental benefits, generate electricity in an irregular way and thus have a poor adaptability to the power grid demand. In such scenario, hydropower plants are becoming more important due to their ability to provide flexibility to the electric power system. It is out of question, then, that hydropower will play a big part in the future of energy generation [1]. To adapt to this increasingly fluctuating power need, turbines are required to respond faster to the grid demands and to undergo more frequent starts and stops. These harsher operating conditions have increased the action of the hydraulic forces on the structure of the turbines, which are more prone to suffering damage. Therefore, it is becoming more and more important to have a deep understanding of the structural response of hydraulic turbines when in operation.

Pelton turbines are among the most important types of turbines used in hydropower. They are action-type turbines with an efficiency that can exceed 90% over a wide operating range, thus being one of the most flexible types of turbine. They are installed in locations with high hydraulic heads, usually above 400 m, and operate with low discharges. The most powerful Pelton turbines are housed in the Bieudron power station in Switzerland, with three units operating under a maximum head of 1883 m and with a rated output of 423 MW each [2]. In Figure 1, a sketch of a horizontal Pelton turbine with two jets is represented. The main component of a Pelton turbine is the runner, which is a circular structure with several bucket-shaped pieces attached along its periphery. The role of the runner is to convert the hydraulic energy into mechanical energy by the impulse of the water. To do so, one or more nozzles are installed at the end of the penstock and directed tangentially to the runner. These convert almost all of the potential energy of the water into kinetic energy. The water comes out of the nozzles as a high-speed jet, which impinges the buckets of the runner perpendicularly. To take full advantage of the kinetic energy of the water, the buckets divide the jet into two nearly symmetrical streams thanks to a middle ridge and deflect them almost 180 degrees. The impulse performed on the buckets is then transmitted to the disk and finally to the shaft [3].

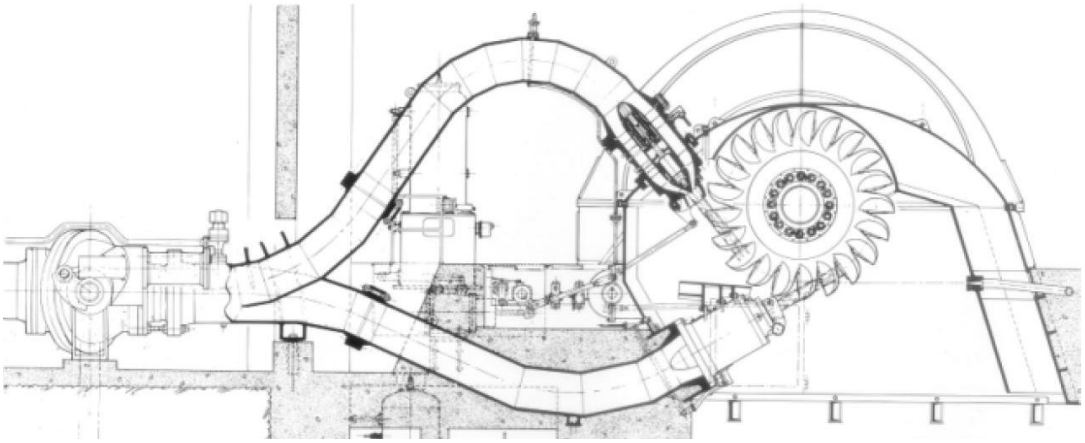

Figure 1. Cross section of a Pelton turbine

Pelton runners may suffer different kinds of failures due to the continuous action of the water jets. The high velocity of the water particles may lead to cavitation pitting,

especially when there are small imperfections on the inner surface of the buckets or the design is not accurate enough [4]. In case of sand-laden water, the erosion of the bucket can become a serious problem and sometimes damage can be catastrophic [5][4]. However, the most severe failures in Pelton turbines arise due to the fatigue of the material. The runner, and especially the buckets, undergoes very strong dynamic forces every time it is impinged by a water jet. This strong bending force is applied at a high rate, which is proportional to the rotational speed, the number of buckets and the number of jets. Since the structure of a bucket is similar to a cantilever beam, most of the stress is condensed at the base of the buckets, what makes it a critical part of the runner and prone to developing cracks. In case of wrong design or faulty casting of the buckets (which can leave imperfections in the material), the service life of the runner can be significantly reduced.

The effect of the water jets can be largely aggravated when the runner structure responds dynamically to these forces. This is known as resonance and happens when the frequency and distribution of the excitation force, i.e. the impingement of the jets, is near a natural frequency and mode shape of the runner. When this stage is reached, the deformation of the runner, especially in the bucket area, is amplified and the stresses largely increased. Therefore, it is crucial to avoid the resonance of the runner, and to do so, the modal behavior and excitation characteristics must be acutely analyzed when designing a new turbine [6]. After commissioning, to have a deep knowledge of the dynamics of the machine also makes it possible to monitor the state of the runner without needing to disassemble [7]. For all these reasons, the modal analysis of Pelton turbines is of paramount importance to ensure a long service life of the machines.

1.1. Modal behavior of Pelton turbines

Many publications can be found about the fluid dynamics of Pelton turbines [8–11]. However, while some papers have been published regarding the structural response of Francis turbines and pump-turbines [12,13], there are a few studies addressing the topic on Pelton runners.

Pelton runners have typically suffered damage in the area of the buckets [14,15]. First, this was attributed to the stresses caused by the centrifugal forces and the impact of the jet, but with the trend to increase the runner size and the concentration of power, the importance of the bucket vibration was also acknowledged. One of the most relevant publications is from Grein et al. [16], who remarked the importance of the dynamic stresses as a controlling parameter for fatigue failure and identified the bucket vibration in circumferential direction as the most dangerous natural mode, whose amplification factor in case of resonance could reach up to x1000.

Some studies described the vibrational modes of Pelton buckets more accurately thanks to the development of Finite Element Methods and with experimental tests in models. Schmied et al. [17] identified the main modes of a Pelton bucket: bending mode in circumferential and axial direction, torsional mode, rim mode and radial mode. It also mentioned that as the number of nodal diameters of the runner increases, so does the resemblance to a pure bucket mode. Other authors, like Pesatori [18] and Sanvito [19], conducted simulations and experiments on buckets of a model runner and identified the mode shapes of the bucket but with limited boundary conditions. The influence of the

disk and mounting position was not considered and only the natural frequencies with higher number of node lines were determined.

A few studies can be found which used numerical models to assess the modal behavior and the stresses beared by prototype runners [20,21]. Nevertheless, the information is not discussed in detail. Angehrn and Dubas [22] carried out the modal and stress analysis of a 260 MW prototype runner, but mainly discussed the stress distribution endured by the structure.

In recent years, some authors have still addressed the dynamic behavior of Pelton runners. Mack et al. [23] performed a numerical and experimental study on a laboratory model to see the influence of water and mass variations on the natural frequencies of the runner. However, the study only focused on the circumferential bending modes and the influence of the shaft wasn't described. In other publications, numerical models of Pelton runners have been used to analyze some failures [24,25], but a detailed explanation of the runner modes is not provided.

In a nutshell, there are no publications providing a comprehensive analysis of the modal behavior of Pelton runners. The main bucket modes have been described, but the effect of attaching the buckets to the disk and the runner to the shaft is still to be discussed. In addition, most of the studies have relied on the use of numerical models and/or reduced scale models, but the modal analysis of real prototypes has not yet been published.

In this paper, the modal response of different Pelton turbines has been evaluated. Four different prototype runners were available to perform experimental tests. In the first part of the study, a numerical and experimental investigation of one of the prototype turbines has been carried out in a systematic way to determine the influence of the different components of the turbine. The study begins with the identification of the main modal shapes of a single bucket using Finite Element Method (FEM). Then the modal shapes and natural frequencies of the whole runner without any constraints are analyzed with another FEM numerical model. The results obtained are validated with experimental tests. At the end, the influence of every component of the turbine is discussed. In the second part of the study, another prototype installed in the same power plant (same operating conditions) but with some differences in the mechanical design has been analyzed experimentally to determine the variation in the frequencies between runners of the same specific speed n_s. Finally, the modal behavior of two other turbines belonging to different power plants (different n_s) is evaluated.

2. First Pelton turbine investigated

The first Pelton turbine is located near a mountainous site in Catalonia (Spain). The machine has a horizontal setup with two equal runners attached on both ends of the shaft and is supported by two bearings (see Figure 2). Each runner is operated by a single jet arranged below the machine in horizontal direction. The characteristics of the turbine are listed in Table 1. To perform the first study, a new prototype runner was available outside the machine, hanging from a rope. Thanks to a 3D scanner, the geometry of the runner was virtually reproduced. From now on, this prototype will be referred to as 1-A.

Figure 2. View of the Pelton unit

Rated head	770,45 m	**Nozzles**	2
Rated output	35 MW	**Jet diameter d_j**	170 mm
Speed	600 min^{-1}	**Specific speed n_s**	19
Runners	2	**Groups**	2

Table 1. Characteristics of the turbine

The geometry of a Pelton runner is quite complex, especially the buckets. They must be shaped to have maximum hydraulic efficiency, but also must guarantee enough structural resistance to bear the forces applied to them during operation. Hence their design must be a compromise between a hydraulic and a structural optimal shape. However, the characteristics of a Pelton turbine are usually represented by two principal dimensions: the pitch diameter D_1, which is defined as double the minimum distance between the axis of the water jet and the runner axis, and the bucket width b. The ratio between these two values is related to the specific speed of the turbine, and thus to the head. A sketch of a Pelton bucket is shown in Figure 3 and the characteristics of the studied runner are listed in Table 2.

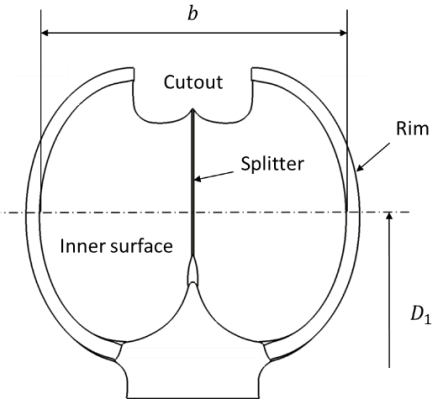

Figure 3. Main dimensions of a Pelton runner

Pitch diameter D_1	1900 mm
Bucket width b	547 mm
No. of buckets	22
Ratio b/D_1	0,288
Material	Stainless steel Cr/Ni 13/4
Year of construction	2016

Table 2. Characteristics of runner 1-A

3. Modal analysis of a Pelton bucket

3.1. Numerical model

The first step consisted in analyzing numerically the modal shapes of a single bucket. The CAD geometry of the bucket was obtained from the 3D scanned model of the runner and the simulation of the modal behavior was then carried out by means of Finite Element Methods. The software used to this effect was the Modal module from ANSYS® W [26]. First, the geometry of the bucket was meshed with 25000 elements after performing a mesh sensitivity analysis. The areas with sharper edges and highest curvatures, such as the cutout or the base of the middle ridge, had a more refined mesh.

In order to analyze the pure bucket modes without the effect of the disk, the boundary conditions for this simulation were to fix the area connected to the rest of the runner (see the green areas in Figure 4). The x-direction corresponds to the tangential direction of the runner, y-direction to the radial and z-direction to the axial direction. The main characteristics of the numerical model are listed in Table 3.

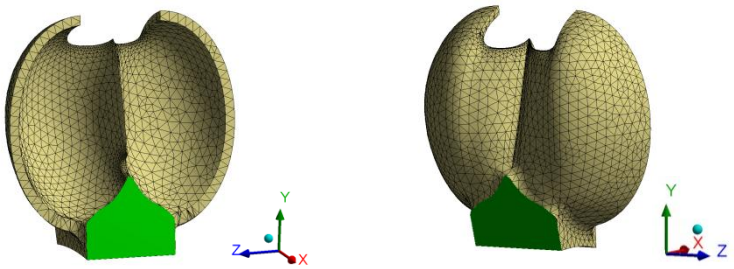

Figure 4. Front and rear view of the meshed bucket

Table 3. Characteristics of the bucket model

Conditions	Fixed base
Material	Stainless steel
Density	7500 kg/m^3
Young's modulus	2x10^{11}
Type of mesh elements	Tetrahedral
Number of mesh elements	25000

3.2. Mode shapes description

Front and side views of the first eight mode shapes are displayed in Figure 5. The areas with minimum displacement are represented in blue and the ones with maximum displacement are represented in red. It is worth noting that the color scale is not the same in all the pictures, since the program takes as a reference the maximum and minimum values of every mode. The shape of the bucket without deformation is depicted with the light wired figure. The first group of modes can be related to the first natural mode of a cantilever beam, in which the structure tilts over the clamped base. In the first and the second one, the bucket bends in the axial and tangential direction of the runner, respectively. The bucket axial mode is found in the lowest frequency because the stiffness is lower in the axial direction than in the tangential direction. For both mode shapes the tips of the bucket deform in phase. In the third mode, or counter phase tangential mode, the bucket halves bend tangentially in opposite phases, thus giving certain torsion around the radial axis of the bucket. In this mode shape we can also see that the splitter is deforming. The fourth natural mode involves the deformation of the rims of the bucket, which deform in the axial direction in counter-phase, spreading and contracting.

The following four modes are featured by the appearance of transversal nodes on the bucket, what increases the stiffness, and thus the frequency. In the fifth and sixth modes the tips of the bucket deform in the radial direction, with the same and opposed phases on both sides, respectively. The deformation of the rims in the axial direction is also

relevant. The seventh mode is similar to the sixth mode, although it combines axial and radial deformation of the tips and has a large twist in the splitter. In the eighth mode two transversal nodes appear and the bucket tips deform in the radial direction. Since the main dimensions of a bucket are standardized in relation to the jet diameter, we can assume that the modes found in this case are representative of most Pelton runners, with slight design variations, such as the attachment of ribs at the rear side of the buckets to increase bending stiffness.

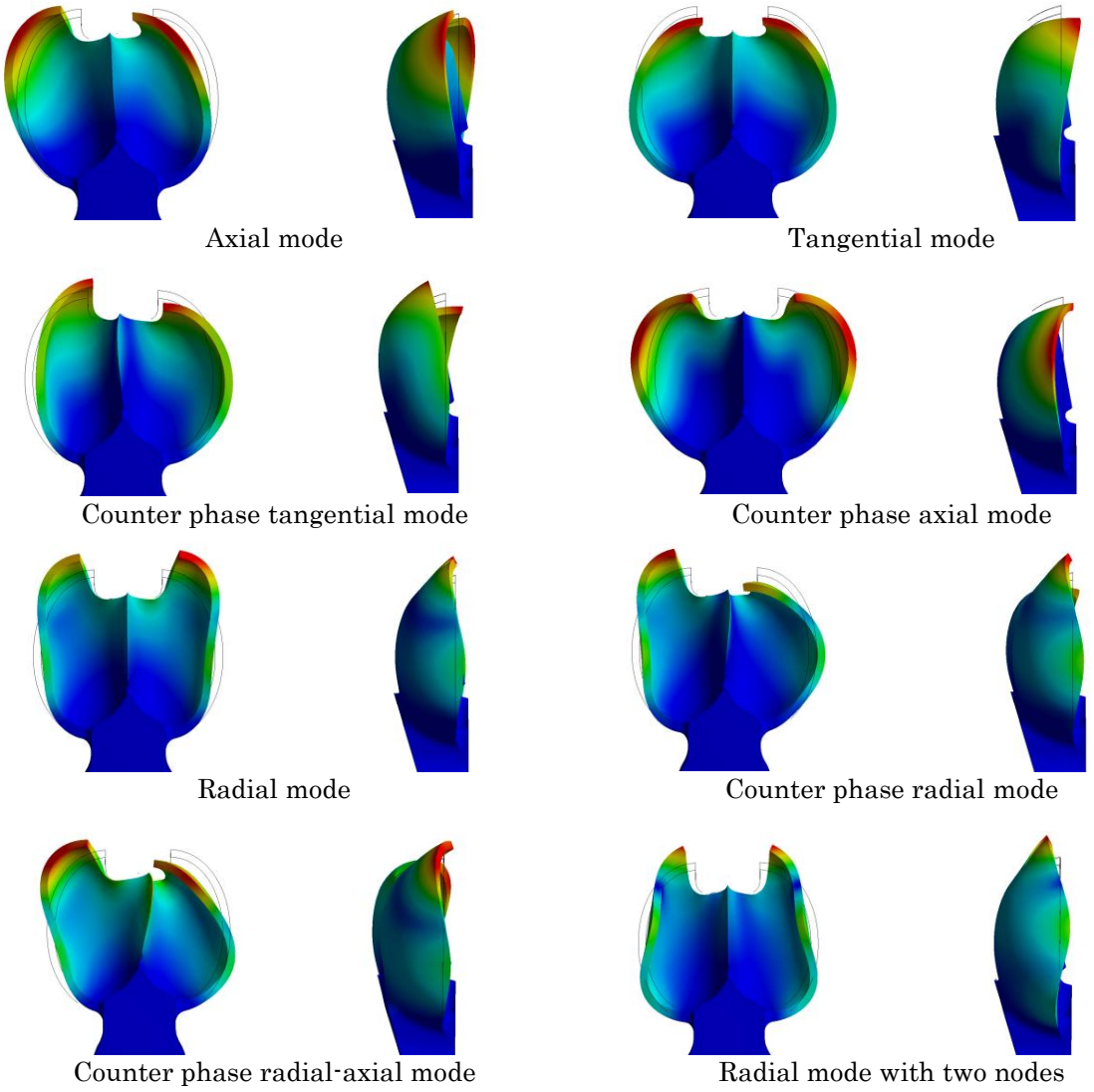

Figure 5. Pure bucket modes

4. Modal analysis of the Pelton runner

4.1. Numerical model

After performing the analysis of a single bucket the modal simulation of the whole runner was carried out. The software used was the same as the single bucket simulation. A mesh sensitivity analysis was done prior to the investigation to ensure a balance between the stability of the simulation results, and reasonable time and computational

resources. The mesh density was increased in the sharp edges and the locations were typically a high concentration of stresses occur. Since the object of this simulation was to understand the modal behavior of the runner without the effect of the shaft, the boundary conditions for this model were setting the structure as a free body, which means that the runner had no constraints. The main characteristics of the final runner model are listed in Table 4. Two views of the mesh are displayed in Figure 6.

Conditions	Free body
Material	Stainless steel
Density	7500 kg/m^3
Young's modulus	2x10^{11}
Type of mesh elements	Tetrahedral
Number of mesh elements	400000

Table 4. Information about the simulation of the runner

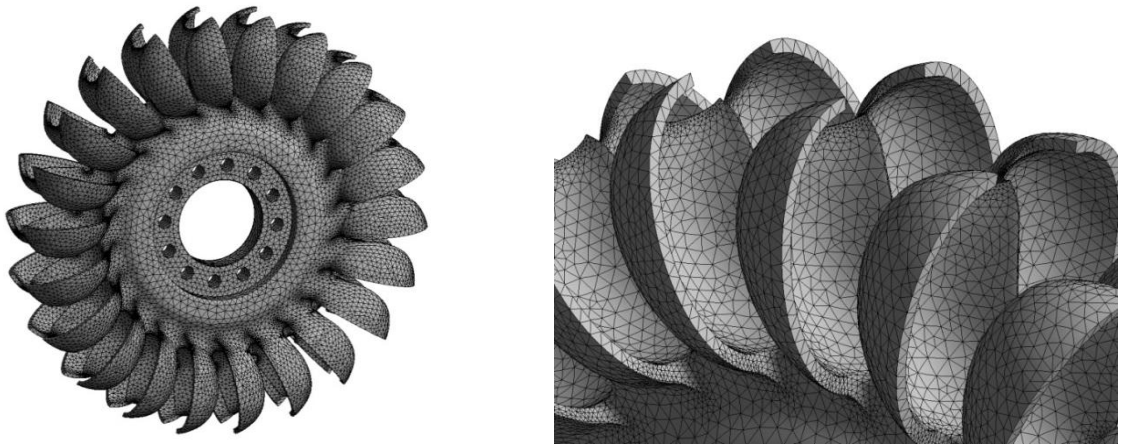

Figure 6. Left: Mesh of the whole runner, right: detailed mesh of the buckets

4.2. Mode shapes description

The simulation shows that the runner has several variants of every bucket mode shape, in which both the wheel and the buckets deform. Every variant is featured by a certain number of nodal diameters of the wheel. These nodal lines delimit the runner areas that vibrate in opposite phases, and between them the buckets and the disk have maximum deformation. The buckets located on the nodal diameters do not deform. It is worth noting that as the number of nodal diameters increase, so does the vibrational frequency of the structure. There is a total amount of 22 modal shapes, which reach a maximum number of 11 nodal diameters.

The axial, tangential and counter phase tangential modal shapes of the Pelton runner with two (2-ND), five (5-ND) and ten (10-ND) nodal diameters are displayed in Figure 7. The order of appearance of the mode shapes is the same as in the pure bucket modes. In the first place, one finds the axial modes, where wheel and buckets are deforming in the axial direction. When the number of nodes increases, the deformation of the disk is minimized and only a deformation in the area of the buckets is noticed. In that case the

maximum deformation, which is found at the tip of the buckets, is increased with respect to lower ND modes. The second group corresponds to the tangential modes. The disk deforms in the radial direction for the first ND modes, while for higher ND only the bending of the buckets is significant, just like in the axial case. In the third group, the counter phased tangential mode involves the movement of the bucket tips in opposite phases. In this case there is no deformation of the disk in the 2-ND, and the maximum deformation of the tips of the buckets is kept almost constant for different ND, unlike the previous cases.

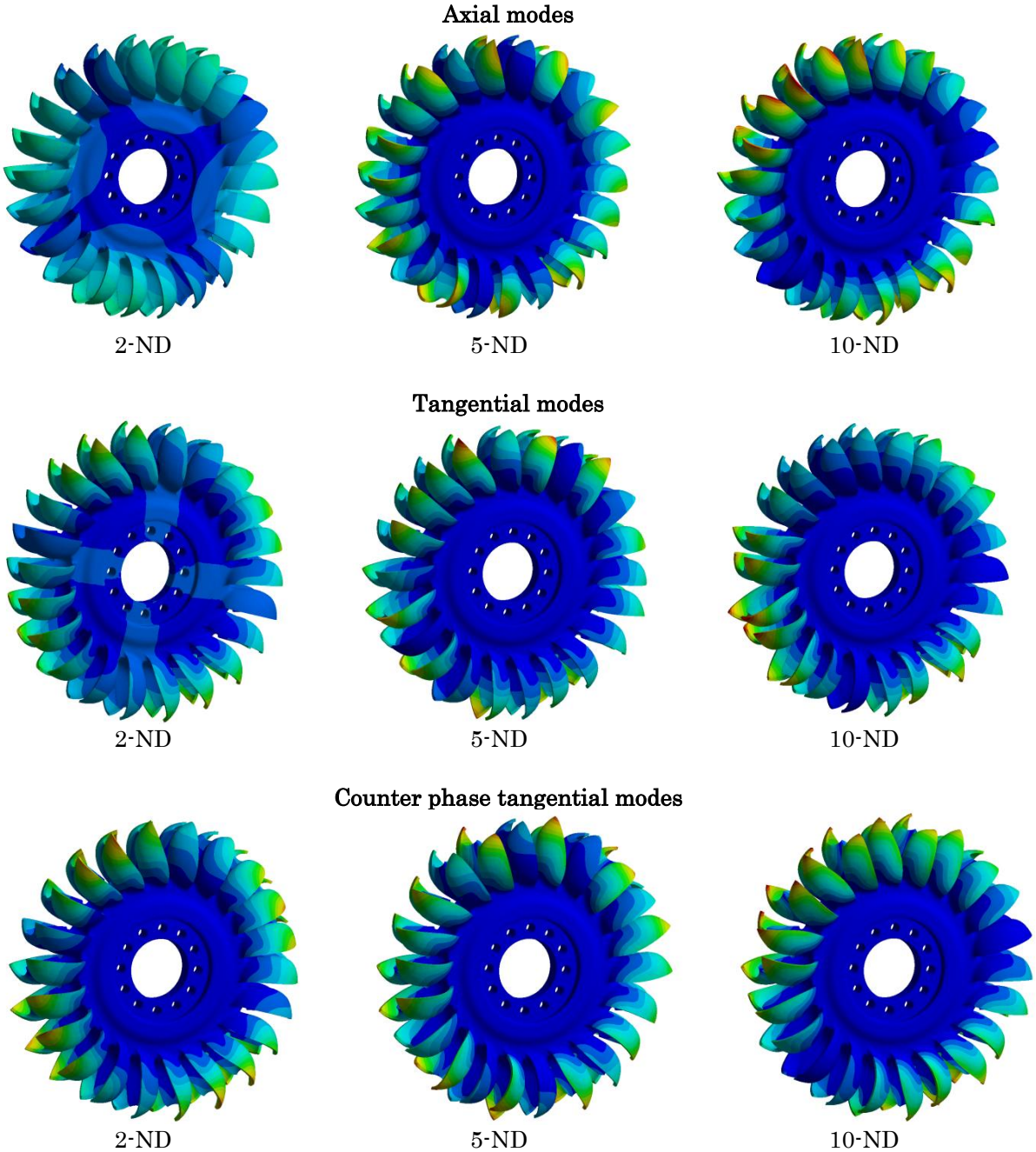

Figure 7. Runner modes

In Figure 8 the next four modes of the Pelton runner are displayed also for 2-ND, 5-ND and 10-ND. One can clearly identify the 2-ND runner deformation in all of them, except in the radial mode, in which the deformation in the disk is much lower than in the

253 buckets. In the counter phase axial modes, the deformation of the disk is in the radial
254 direction, while in the counter phase radial mode it is in the axial direction. In all of
255 them, the deformation of the tip/rim of the buckets increases with the number of nodal
256 diameters.

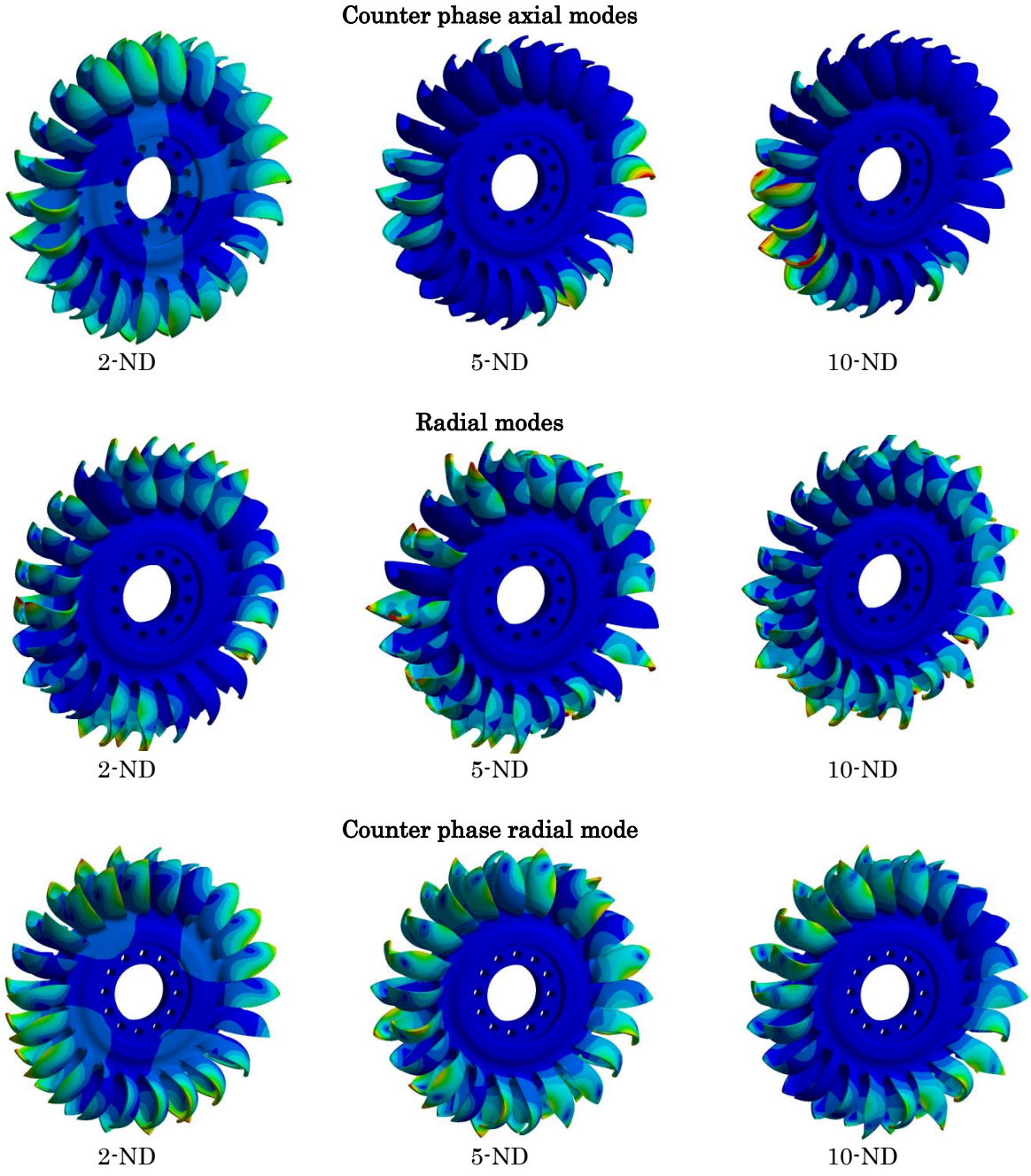

Figure 8. Runner modes 2

257 ### *4.3. Experimental study*

258 The numerical results were validated by performing an Experimental Modal Analysis
259 (EMA) in the prototype. The first experimental test was addressed to studying the pure
260 mode shapes and frequencies of the Pelton runner, without the influence of the rotor.
261 Therefore, the runner was suspended with a rope and placed in an accessible location of
262 the power station to carry out impact tests. This was equivalent to considering the

runner as a free body (without any constraint) due to the small influence of the rope on the vibration of the runner. The procedure consisted in doing impacts with an instrumented hammer on different locations of the structure and in recording the vibrational response with different sensors. The ones used in this experiment were industrial K-Shear® accelerometers from KISTLER type 8752A50. Their sensitivity was 100 mV/g and the acceleration range ±50 g. They were mounted on clean and flat locations of the runner to ensure reliable and accurate measurements. The hammer had a sensitivity of 223 μV/N.

To perform the EMA the location of the sensors was chosen accurately to represent the main mode shapes of the runner. Four accelerometers were placed on the surface of the disk (axial direction) with approximately 90 degrees between them and the same radial position. Moreover, four accelerometers were placed on different locations of the buckets to detect the axial, tangential and radial modes. The axial accelerometers were adhered on the outer surface of the bucket rim, approximately in the middle section, and the tangential and radial accelerometers were placed on the tip of the bucket, on perpendicular surfaces. Since the vibration of a runner is complex, different series of impacts were carried out. In each series the accelerometers were relocated in different parts of the buckets. One distribution to detect tangential modes of the runner is displayed in Figure 9.

Figure 9. Accelerometers disposition on the hanged runner

The vibration time signal was transmitted to a recording module LAN-XI Data Acquisition Hardware from Brüel & Kjær. The recorded time signal was later converted into an acceleration-frequency signal (spectrum) by performing a Fast Fourier Transformation (FFT). The time-force signal from the instrumented hammer was also transmitted to the acquisition module and was later used to perform a Frequency Response Function (FRF) with the signal from the accelerometer. The FRF divides the accelerometer signal by the hammer signal thus representing the excitability of the structure, regardless of the force magnitude. An Operational Deflection Shape (ODS) was created to identify the modal shapes of the runner for every natural frequency (see Figure 10 left). The frequencies were obtained by peak picking from the FRF of different sensors. In Figure 10 right the FRF of one accelerometer can be seen. The lower chart is the amplitude of the acceleration/force ratio and the upper chart is the phase difference between the accelerometer and hammer signal. Two representations of tangential mode shapes are displayed in the graph; 1-ND on the left and 4-ND on the right.

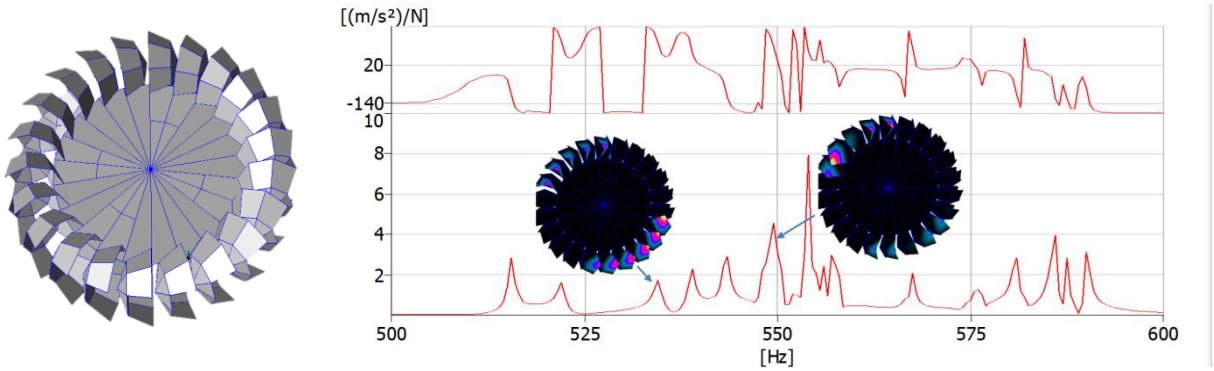

Figure 10. Left, ODS model of the Pelton runner; right, FRF and ODS mode shapes of experimental impacts

In Table 5, the axial natural frequencies obtained from the experimental tests are compared to the frequencies obtained with the numerical model. In Table 6, the same comparison is shown for the tangential frequencies. It can be seen that the mode shapes of the real runner correspond to the ones of the numerical model and for all the frequencies the error is less than 2%. With this, it is proved that the numerical model created is validated because it represents well the real prototype behavior.

	2-ND	**3-ND**	**4-ND**	**5-ND**	**6-ND**	**7-ND**
Exp. [Hz]	195,5	356	424	449,5	461	466,5
Num. [Hz]	194,3	353,9	423,1	449,4	461,1	467,1
Rel. error [%]	< 1%	< 1%	< 1%	< 1%	< 1%	< 1%

Table 5. Comparison of runner axial frequencies between simulation and experiment

	2-ND	**3-ND**	**4-ND**	**5-ND**	**6-ND**	**7-ND**
Exp. [Hz]	517	541,75	547,5	549	550,7	552,25
Num. [Hz]	519,3	545,6	551,97	554,87	556,32	557,09
Rel. error [%]	< 1%	< 1%	< 1%	1,07%	1,02%	< 1%

Table 6. Comparison of runner tangential frequencies between simulation and experiment

5. Results and discussion

This section attempts to analyze the modes of a Pelton runner by comparing the vibrational modes of the wheel with those of a single bucket. The interaction between both elements will be studied in order to have a better understanding of the modal behavior of the turbine. In Figure 11, the frequencies obtained from the numerical model (upper chart) can be compared with the experimental results (lower chart). Every type of bucket mode shape is attributed a color to relate more easily the peaks from the experimental tests with the numerical modes. The modes studied are located in a range between 0 and 1200Hz. The first modes found are the axial modes between 195 Hz and 473 Hz. They are followed by the tangential modes (in phase and counter phase), which appear between 519 and 591Hz and overlap each other. Next the counter phase axial modes are found in a very narrow frequency range between 618 and 648 Hz. The counter phase radial modes and the radial modes are found in the next frequency band, being the former ones spread over a wide range of frequencies and the latter concentrated in a

narrow band (1017 to 1077 Hz). Similar to the counter phase axial modes, the counter phase radial-axial modes have small differences between them.

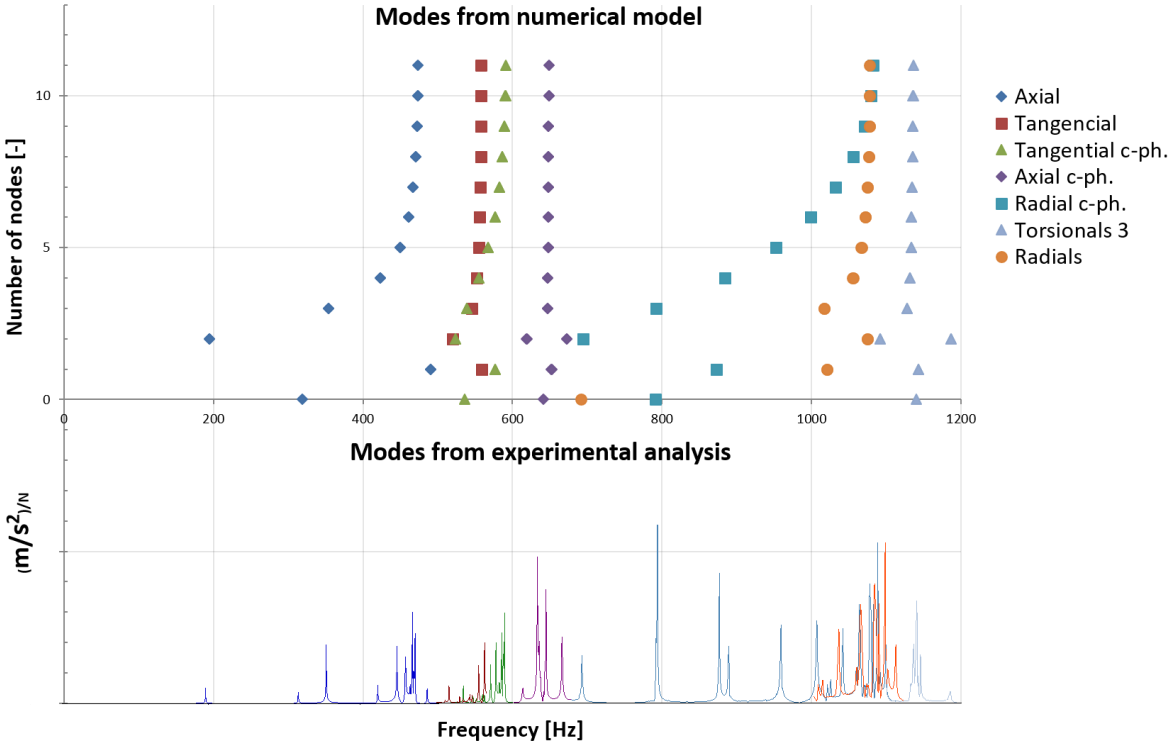

Figure 11. Numerical and experimental modes of a Pelton runner: a) Numerical results, b) Response spectrum after the impacts

5.1. Analysis of the coupling between the disk and the buckets

A noticeable fact is the nonlinear increase of the frequencies, which are distributed in a similar way to an asymptote. The modes in lower frequencies are those with a fewer number of runner nodal diameters. As the number of nodal lines increases, so does the frequency, but at a decreasing rate. For instance, the axial mode with 2 ND has a frequency of 194,3Hz and the one with 3 ND a frequency of 353,9Hz, which is about 82% of increase. However, the 4-ND mode is found at 423,1Hz, which is less than 20% increase with respect to the 3-ND mode. After 5-ND, frequencies converge in a small range, with a frequency variation lower than 3%. This effect is caused by the interaction between the modal shapes of the disk and the modal shapes of the buckets.

To appreciate the contribution of every component to the global modal shapes of the turbine, three simplified models have been studied: a disk (model 1), a disk with a single peripheral mass (model 2) and a disk with separated peripheral masses (model 3). The distribution of frequencies can be seen in Figure 12. In model 1, the frequencies increase steadily with the number of nodal diameters. This is attributed to the fact that the mass oscillating between the nodal diameters becomes more restricted, thus having an increase in the stiffness. Attaching a peripheral mass to the disk (model 2) increases the overall stiffness of the modes. However, when it comes to the disk with attached masses (model 3), the frequencies change their distribution. The maximum frequency is lowered. We can say that for a fewer number of nodal diameters the modes are governed by the disk (the frequencies are very similar for both models) while for an increased number of nodal diameters, the modes become more dominated by the masses.

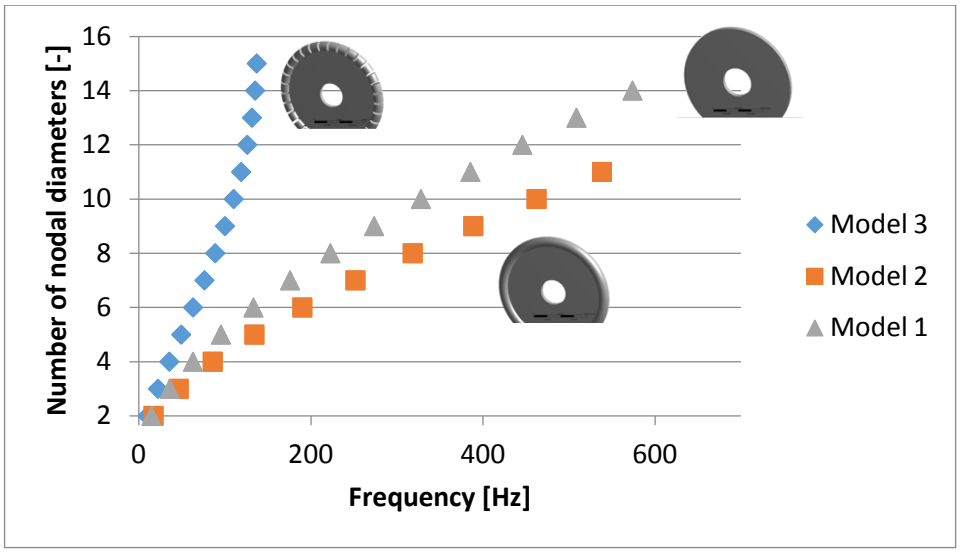

Figure 12. Frequencies of a disk and of a disk with masses

To see the progression from a disk-dominated mode to a bucket-dominated mode the deformation of the outer diameter of the disk in the axial direction in model 1 and model 3 has been represented in Figure 13. It can be seen that in model 1 the maximum displacement is kept almost constant. This fits the behavior observed in the distribution of frequencies: the modal mass is kept almost constant, and the frequency increases steadily due to the stiffness increase. However, in model 3 the deformation of the disk decreases largely between 2 ND and 4 ND. From 5 ND the deformation barely shows a reduction. Some conclusions can thus be extracted from the chart. First, the increase in disk nodal diameters from 2 ND to 4 ND happens to reduce largely the vibrating mass of the disk, which explains the large difference between the first frequencies. Second, for modes higher than 5 ND the deformation of the disk is very small and shows almost no variation, even if the number of nodal diameters is increased. It can be said then that in the higher modes almost all the vibration is performed by the buckets, and that their base is similarly restricted, what help explaining why all the frequencies are so similar. Therefore, when studying the runner, the mode in the highest frequency, which corresponds to 11 ND, has the most resemblance to a pure bucket mode. The base of the bucket has the smallest angle between nodal diameters, being the most rigid one.

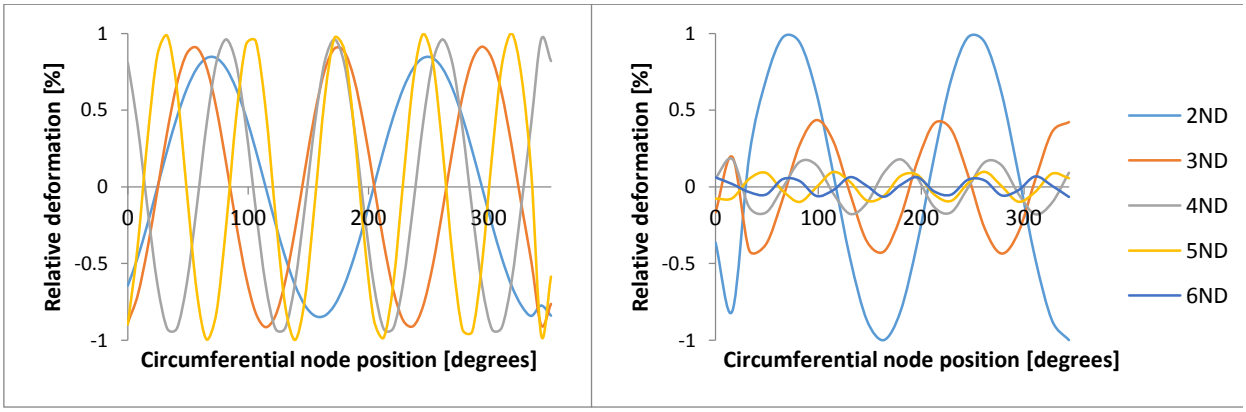

Figure 13. Relative deformation of the outer periphery modes in: left, the disk and right, the disk with masses

To check the similarity of the 11-ND mode to a simple bucket vibration, another analysis has been performed. The natural frequencies of a single bucket and the natural frequencies obtained in the 11-ND runner mode are indicated in Table 7. The frequencies are similar, with less than 4% of difference. It is worth noting, though, that this variation differs from one bucket mode shape to another. The axial and the counter phase radial mode shapes are the most affected by the change in the boundary conditions of the disk.

	Single bucket [Hz]	Runner mode 11ND [Hz]	Rel. difference [%]
Axial	487,8	473,7	2,98%
Tangential	564,9	558,2	1,20%
Tangential c-ph.	590,9	591,2	0,05%
Axial c-ph.	635,0	648,6	2,10%
Radial c-ph.	1120,4	1082,3	3,52%
Radial	1091,9	1077,9	1,30%

Table 7. Variation in the bucket frequencies for different modes

5.2. Effect of the bucket mode shapes

As indicated above, the effect of the coupling to the disk affects differently on every bucket mode. Some of them converge in a small range, like tangential and counter phase axial modes. Such behavior can be attributed to the nature of the deformation of the bucket and its interaction with the disk. Some modes imply a low contribution of the disk, for example the counter phase axial modes, which are very local and only affect the rim of the buckets. For these types of modes, a change in the stiffness of the coupling to the disk doesn't affect much the vibration of the buckets. On the other hand, it is also important to mention that the increase in the number of nodal diameters affects basically the stiffness in the axial direction. In circumferential and radial direction, the disk is very stiff, regardless of the number of nodal diameters. Therefore, the modes with a large axial deformation of the disk (see axial and counter phase radial in Figure 7 and Figure 8) are more sensitive to the disk stiffness variation. Tangential and counter phase axial modes have a significant deformation of the disk but in the radial direction. In Figure 14 the deformation of the runner of 2-ND mode shapes at the base of the buckets in the axial direction has been plotted. It is clear that the axial and counter phase radials are the mode shapes most influenced by the axial stiffness of the disk.

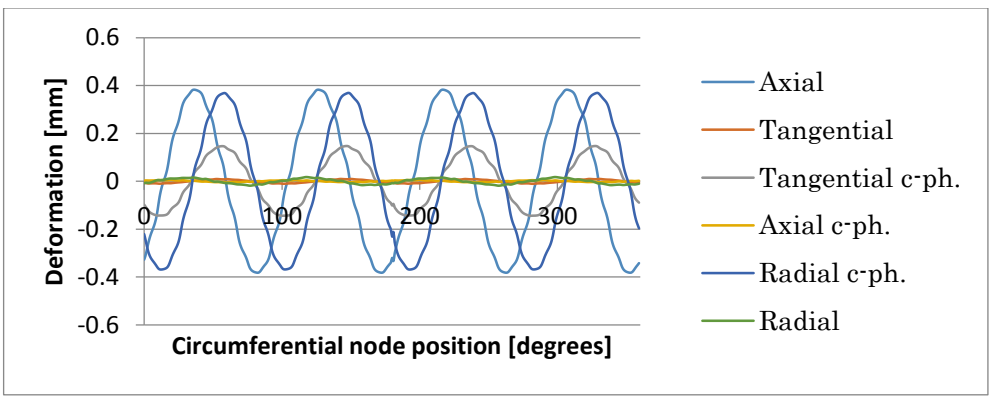

Figure 14. 2-ND axial deformation of the base of the buckets for every mode shape

6. Modal behavior of other Pelton turbines

The main geometrical features of a Pelton turbine are related to its head H, discharge Q and number of nozzles. The specific speed is defined as

$$n_s = \frac{nQ^{0.5}}{E^{0.75}} \quad \text{Eq. (1)}$$

where n is the rotational speed of the turbine, Q the discharge and E the specific energy and is used to classify hydraulic machines. The specific speed n_s is related to the head of the turbine and, for Pelton, this is connected to the ratio between the runner diameter and the jet diameter D/d_j. In like manner, the discharge of the turbine is related to the dimensions of the bucket. Thus the dimensions of a Pelton runner (from the hydraulic point of view) are characterized by the specific speed n_s. However, even for the same n_s, runners may bear some differences, especially in the structural design, depending on the manufacturer and on the year of construction.

So far, the modal behavior of Pelton turbines has only been studied for a single case. To determine to which extent the results are representative of other turbines, a runner with the same basic dimensions and characteristics as the one studied previously is analyzed in order to determine how the modal behavior may vary between designs with the same hydrodynamic features. Afterwards, other runners with different specific speeds will be analyzed and compared.

6.1. Influence of the structural design for runners with the same n_s

The runner studied in this section is located in the same power plant and has the same features of runner 1-A (listed in Table 2). The runner is connected to the rest of the machine. However, the mechanical design is different. This prototype will be referred to as 1-B. Figure 15 left shows a view of the turbine 1-B with the casing disassembled.

Figure 15. Left, runner 1-B attached to the machine and left, accelerometers placed on one bucket

An experimental modal analysis was carried out to determine the modal shapes and frequencies of the runner. The procedure and the instrumentation were the same described in the experiment of prototype 1-A. Impacts in the axial, radial and tangential

direction were performed on all the accessible buckets and the natural frequencies and corresponding mode shapes were identified. A picture of the accelerometers during the impact tests is shown in Figure 15 right.

The experimental results of runner 1-B are presented in Figure 16. It is seen that the runner mode shapes appear in the same order as the runner 1-A. The modes with fewer nodal diameters (dominated by the deformation of the disk) have lower frequencies than the modes with more nodal diameters (dominated by the bucket). As seen in the previous results, the axial and counter-phase radial modes are also the most affected by the stiffness of the disk, because of the difference between the frequencies of 2-ND and 11-ND. The distribution is asymptotic as well. However, the natural frequencies of runner 1-B are higher than 1-A.

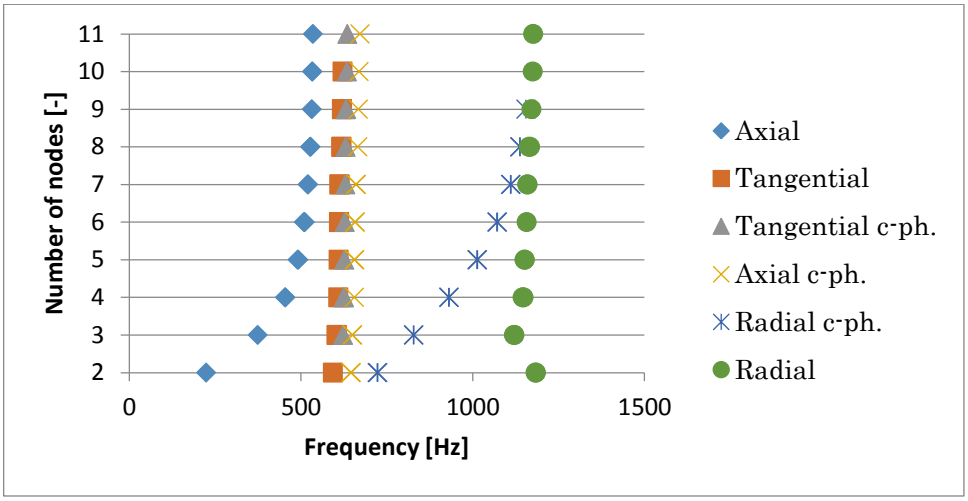

Figure 16. Left, natural frequencies of an old runner with buckets with ribs and right, view of the runner

In Table 8, the axial frequencies of runners 1-B have been compared to those of runner 1-A. The frequencies dominated by the deformation of the disk have a difference of less than 2% between both designs. Nevertheless, as the vibration becomes more located in the buckets the difference between 1-B and 1-A increases. The frequencies of the bucket-dominated modes of design 1-B are around 10% higher than 1-A. In Table 9, the difference in tangential frequencies between both designs is also presented. All the modes are affected similarly by the variation in the mechanical design, being the frequencies of runner 1-B around 9% higher than the runner 1-A.

	3ND	4ND	5ND	6ND	7ND	8ND	11ND
Runner 1-B [Hz]	373,5	453,5	489,8	508	519,3	526,3	534,3
Runner 1-A [Hz]	369,8	426,9	450,3	461,3	467,2	470,5	473,7
Rel. diff. [%]	1,0	5,8	8,1	9,2	10,0	10,6	11,0

Table 8. Axial frequencies in the old runner and the new runner

	3ND	4ND	5ND	6ND	7ND	8ND	11ND
Runner 1-B [Hz]	603,3	608,1	609,1	610,1	611,4	617	620,6
Runner 1-A [Hz]	550,8	553,1	555,5	556,5	557,2	557,6	558,2
Rel. diff. [%]	8,7	9,0	8,8	8,8	8,9	9,6	10,1

Table 9. Tangential frequencies in the old runner and the new runner

From the previous analysis, it can be deduced that the mechanical design mainly affects the frequencies dominated by the vibration of the buckets. The difference between runners of the same hydraulic design can be up to 10%. This variation is mainly due to the shape of the buckets. The buckets of runner 1-A and runner 1-B are represented in Figure 17. The design is different, especially in the back area. The buckets of the older runner design (1-B) are supported by ribs in the rear side in order to increase the stiffness and the resistance to the impacts of the jet. The new runner design (1-A), though, does not have these supports and has a more polished shape. This design variation has a large effect on the natural frequencies. It can be thus concluded that for prototypes with the same hydrodynamic characteristics, only the disk dominated modes can be expected to be similar. The bucket-dominated modes change due to a variation of the rear design, and with the less supported buckets of new designs, the bucket-dominated modes can be significantly reduced.

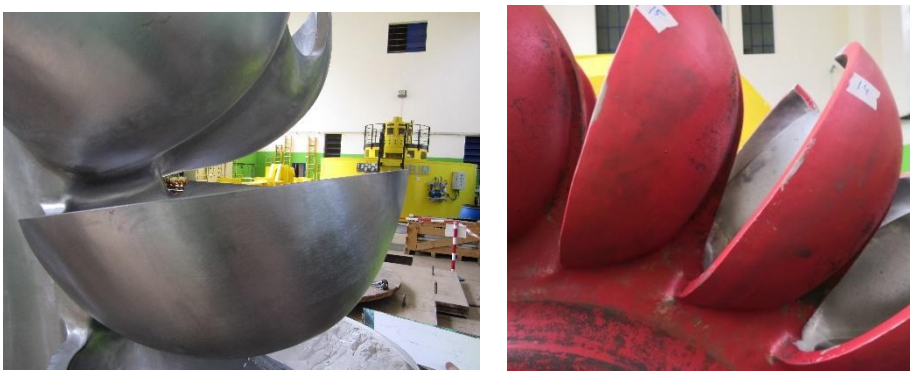

Figure 17. Left, buckets of runner 1-A and, right, buckets of runner 1-B

6.2. Influence of the structural design for runners with different n_s

In the previous section, the modal behavior of two Pelton runners with the same dimensions and hydraulic design has been studied. To see if this can be extrapolated to other machines, the modal behavior of a prototype Pelton turbine with a different hydraulic design has been studied experimentally (see Figure 18). The information regarding the turbine and the runner, which will be referred to as runner 2, is listed in Table 10 and Table 11 respectively. The procedure followed to identify the natural frequencies and the modal shapes was similar to the one described for the first studied turbine.

Figure 18. View of the Pelton unit 2

Rated head	556 m	**Nozzles**	2
Rated output	12 MW	**Jet diameter d_j**	135 mm
Speed	600 min^{-1}	**Specific speed n_s**	17
Runners	1	**Groups**	3

Table 10. Characteristics of Pelton turbine 2

468

Pitch diameter D_1	1500 mm
Jet diameter d_j	135 mm
Bucket width b	427 mm
No. of buckets	21
Ratio b/D_1	0,285
Material	Stainless steel Cr/Ni 6/4

469 Table 11. Characteristics of runner 2

470 The results obtained after the impact tests are represented in Figure 19. The natural
471 frequencies of this prototype are higher compared to the prototype 1-A and 1-B because
472 of the reduced size of the runner. Nevertheless, the order of appearance of the runner
473 mode shapes is the same, even though the dimensions are different. The lowest
474 frequencies correspond to the axial mode shapes of the runner, and these are followed by
475 the tangential and axial counter-phase modes. Regarding the distribution of frequencies,
476 the axial and the radial counter-phase modes are the most affected by the stiffness of the
477 disk and show an asymptotic transition from disk-dominated modes to bucket-dominated
478 modes. In this case, though, also the radial in-phase modes interact with the disk, while
479 in the other prototypes this mode shape wasn't affected by the stiffness of the base. Since
480 the mode shapes of the bucket become more complex at higher frequencies, the similarity
481 between different prototypes is reduced due to the variation in the design. However, the
482 simplest vibration modes of the disk and the buckets (axial and tangential modes) show
483 a similar pattern.

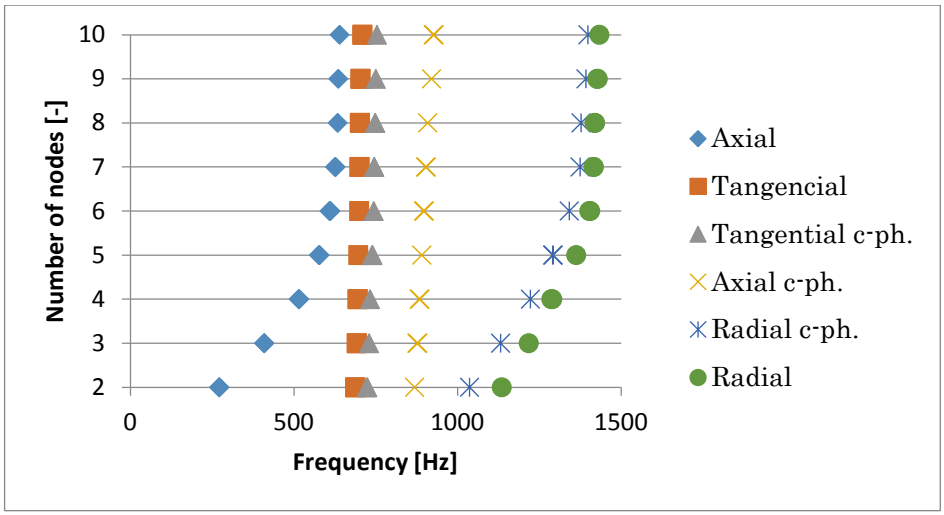

Figure 19. Frequency distribution for Pelton turbine 2

Even though the prototypes studied have similar modal characteristics, they have different dimensions (b/D_1) and sizes. To be able to compare the results between runners with different features, the frequencies have to be represented in a non-dimensional way. In Figure 20, the axial and tangential frequencies of three studied runners have been represented. All the frequencies have been referred to the maximum frequency of the axial modes, the one corresponding to 11-ND, to see if the non-dimensional distribution of the modes and the distance between axial and tangential modes follow the same pattern between different runners. The prototypes represented in the chart are runner 1-B and 2. Moreover, the results obtained from a turbine with a rated head of 800 m (n_s=18), which will be referred to as runner 3, have also been included. The data regarding runner 3 is not disclosed due to confidentiality.

Observing the results in Figure 20, it can be seen that for the three studied runners the relative distribution of natural frequencies is comparable. Regarding the axial modes, the transition from disk-dominated to bucket-dominated modes follows the same asymptotic pattern. The first disk-dominated axial frequency (2-ND) is 30-45% lower than the highest axial frequency (11-ND). Tangential frequencies are around 15% higher with respect to the bucket-dominated axial frequencies in the three cases.

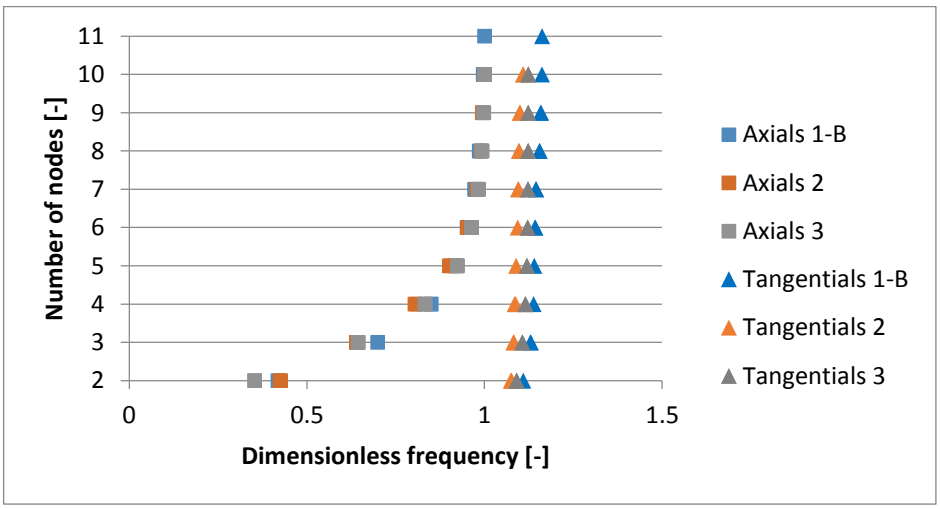

Figure 20. Axial and tangential natural frequencies of several runners in a non-dimensional form

With this information, it can be concluded that for the studied Pelton runners, the modal behavior has very similar characteristics. The simplest vibration modes of the buckets can be compared to the bending of a cantilever beam. Bending in the circumferential direction of the disk is always more difficult for the bucket than bending in the axial direction, so the axial modes are always at lower frequencies than tangential modes. In addition, since the main dimensions of the buckets of a Pelton runner are always relative to their width b (with small differences depending on the manufacturer, year of construction and so on), it is reasonable to expect tangential frequencies to appear near the axial frequencies. Future studies should be aimed at gathering more experimental data from prototypes and at determining how this behavior varies depending on the design, manufacturing process, material and so on.

7. Conclusions

In this paper a detailed study of the modal response of Pelton turbines is presented. Prototypes from different power plants have been analyzed numerically and experimentally for this purpose.

The first part of the study consisted in analyzing in-depth the modal behavior of a Pelton runner without constraints (without being connected to the shaft). The prototype was hanged by a rope in the power plant and fully accessible to perform experimental tests. A 3D scanning of the complete structure was performed to obtain the CAD geometry of the runner. The analysis was carried out following a systematic approach. First, the mode shapes of the bucket were determined numerically. Then, the whole runner structure was analyzed numerically and experimentally. After that, the effects of the interaction between the buckets and the disk were discussed.

The typical modes of a Pelton bucket were classified according to the direction of the deformation and to the number of transversal nodes. In this way, the bucket modes were identified as axial, tangential or radial, and as phase or counter-phase, depending on the phase between the bucket halves.

The analysis of the runner was performed with a numerical model and with a thorough experimental investigation. The results showed that for every kind of bucket mode, the runner has several variants, which are coupled to the modes of the disk (N nodal diameters). For each group of bucket modes, the frequencies increase with the number of nodal diameters of the disk. It was noticed that in lower frequencies the vibration is global to all the runner (behaves like a disk) and in higher frequencies the vibration is more restricted and is dominated by the vibration of the buckets. In addition, some bucket modes are more affected by the stiffness of the disk than others and this affects the distribution of frequencies. For example, tangential modes gather in a small frequency range, while axial modes are more spread. The natural frequencies of the whole runner are lower than the ones obtained with a fixed single bucket.

The second part of the study consisted in determining the effect of structural design in turbines with the same hydrodynamic characteristics. For that purpose, an experimental modal analysis was performed in another prototype of the same power plant. The main dimensions and specific speed were the same. The results showed that the mode shapes appear in the same order and that the frequencies are similarly distributed. The

frequencies dominated by the vibration of the disk are similar in both runners. However, the bucket-dominated frequencies vary up to 10%, because of the different bucket design and especially the use of rear supports in the older runner.

In the third part, a prototype with different hydraulic and mechanical characteristics was studied experimentally. The results indicated that the mode-shapes, as well as their order of appearance, are the same. The natural frequencies were distributed in a similar way, except the radial counter-phase modes.

Finally, to overcome the difficulty of comparing turbines with different sizes and dimensions, the axial and tangential frequencies of three runners with different designs were represented in a non-dimensional way. The results showed that the distribution is similar and that tangential frequencies are 15% higher than axial bucket-dominated frequencies. This is reasonable due to the standardized dimensions of the buckets with respect to its width.

Acknowledgements

The authors would like to acknowledge Endesa Generación for providing access to the hydropower plants, especially to Josep Argelaga and Ramon Feixa. In addition, the authors wish to mention Christian Probst and Reiner Mack, from Voith Hydro, for their support and collaboration in this study.

References

[1] L. Gaudard, F. Romerio, The future of hydropower in Europe: Interconnecting climate, markets and policies, Environ. Sci. Policy. (2013) 1–10. doi:10.1016/j.envsci.2013.09.008.

[2] H. Keck, G. Vullioud, P. Joye, Commissioning and Operation Experience with the World's largest Pelton turbines Bieudron, (2004) 1–16.

[3] M. Nechleba, Hydraulic Turbines. Their Design and Equipment, 1957.

[4] H. Brekke, State of the art in Pelton turbine design, Hydropower Dams. (1994) 21–28. doi:10.1016/j.cger.2011.07.002.

[5] A.K. Rai, A. Kumar, T. Staubli, Hydro-abrasive erosion in Pelton buckets : Classification and field study, Wear. 393 (2017) 8–20. doi:10.1016/j.wear.2017.08.016.

[6] M. Egusquiza, E. Egusquiza, C. Valero, A. Presas, D. Valentín, M. Bossio, Advanced condition monitoring of Pelton turbines, Meas. J. Int. Meas. Confed. 119 (2018) 46–55. doi:10.1016/j.measurement.2018.01.030.

[7] P. Dörfler, M. Sick, A. Coutu, Flow-Induced Pulsation and Vibration in Hydroelectric Machinery, Springer, 2013.

[8] A. Perrig, F. Avellan, J.-L. Kueny, M. Farhat, E. Parkinson, Flow in a Pelton Turbine Bucket: Numerical and Experimental Investigations, J. Fluids Eng. 128 (2006) 1–9. doi:10.1115/1.2170120.

[9] B. Zoppé, C. Pellone, T. Maitre, P. Leroy, Flow Analysis Inside a Pelton Turbine

586 Bucket, J. Turbomach. 128 (2006) 500. doi:10.1115/1.2184350.

587 [10] S. Kvicinsky, Méthode d'analyse des écoulements 3D à surface libre: application aux
588 turbines Pelton, École Polytechnique Fédérale de Lausanne, 2002.

589 [11] S. Alimirzazadeh, T. Kumashiro, S. Leguizamón, E. Jahanbakhsh, A. Maertens, C.
590 Vessaz, K. Tani, F. Avellan, GPU-accelerated numerical analysis of jet interference in a
591 six-jet Pelton turbine using Finite Volume Particle Method, Renew. Energy. 148 (2020)
592 234–246. doi:10.1016/j.renene.2019.11.131.

593 [12] E. Egusquiza, C. Valero, A. Presas, X. Huang, A. Guardo, U. Seidel, Analysis of the
594 dynamic response of pump-turbine impellers. Influence of the rotor, Mech. Syst.
595 Signal Process. 68–69 (2016) 330–341. doi:10.1016/j.ymssp.2015.05.034.

596 [13] C.G. Rodriguez, E. Egusquiza, X. Escaler, Q.W. Liang, F. Avellan, Experimental
597 investigation of added mass effects on a Francis turbine runner in still water, 22 (2006)
598 699–712. doi:10.1016/j.jfluidstructs.2006.04.001.

599 [14] A.A. Fulton, Present Tendencies in Water Turbine Machinery, Proc. Inst. Mech. Eng.
600 135 (1937) 387–444. doi:10.1243/pime_proc_1937_135_029_02.

601 [15] A.B. Winterbottom, Cracking of Bucket Lugs in Pelton Turbines, 127 (1951).

602 [16] H. Grein, R. Angehrn, M. Lorenz, A. Bezinge, Inspection periods of Pelton runners, in:
603 n.d.

604 [17] J. Schmied, T. Weiss, R. Angehrn, Detuning of Pelton Runners, Proc. 7th IFToMM
605 Conf. Rotor Dyn. (2006) 25–28.

606 [18] E. Pesatori, G. Turozzi, P. Pennacchi, A. Tosi, Dynamic Investigation on a Pelton
607 Runner: FEM Calculations and Experimental Results, Proc. ASME 2007 Int. Des. Eng.
608 Tech. Conf. Comput. Inf. Eng. Conf. (2007) 3–7.

609 [19] M. Sanvito, L. Coscarelli, E. Pesatori, G. Turozzi, P. Pennacchi, A New Method for the
610 Dynamic Analysis of Pelton Runners Using CFD/FEM Interaction, Proc. ASME 2009
611 Int. Des. Eng. Tech. Conf. Comput. Inf. Eng. Conf. (2009) 1–5.

612 [20] J. Mañanés, A. Mirasso, A. Antunez, Manufacture of the Pelton runners of Pykara,
613 India, Hydropower Dams. (1999) 58–59.

614 [21] J. Vesely, J. Mikulasek, P. Vesely, Modern technologies for producing Pelton runners,
615 Hydropower Dams. (2006) 113–117.

616 [22] R. Angehrn, M. Dubas, Experimental stress analysis on a 260MW Pelton runner, in:
617 Proc. 11th IAHR Symp., 1982.

618 [23] R. Mack, C. Probst, Evaluation of the dynamic behavior of a Pelton runner based on
619 strain gauge measurements, IOP Conf. Ser. Earth Environ. Sci. (2016).
620 doi:10.1088/1755-1315/49/2/022001.

621 [24] J.C. Chávez, J.A. Valencia, G.A. Jaramillo, J.J. Coronado, S.A. Rodríguez, Failure
622 analysis of a Pelton impeller, Eng. Fail. Anal. 48 (2015) 297–307.
623 doi:10.1016/j.engfailanal.2014.08.012.

624 [25] M. Egusquiza, E. Egusquiza, D. Valentin, C. Valero, A. Presas, Failure investigation of
625 a Pelton turbine runner, Eng. Fail. Anal. 81 (2017) 234–244.
626 doi:10.1016/j.engfailanal.2017.06.048.

627 [26] X. Chen, Y. Liu, Finite element modeling and simulation with ANSYS workbench,
628 2014. doi:10.1201/b17284.

629